organics

MDPI

Article

Absorption Spectra of Protonated Corroles: Two Distinct Patterns Due to Peripheral Substitution Architecture

Lev L. Gladkov [1], Dmitry V. Klenitsky [2] and Mikalai M. Kruk [2,*]

[1] Department of Physical and Mathematical Basis of Informatics, Belarusian State Academy of Communications, 8/2, F. Skorina Str., 220114 Minsk, Belarus; llglad@tut.by
[2] Department of Physics, Belarusian State Technological University, 13a, Sverdlova Str., 220006 Minsks, Belarus; klen@belstu.by
* Correspondence: m.kruk@belstu.by; Tel.: +375-17-3994960

Abstract: The origin of individual features in the ground state absorption spectra of two protonated corroles differing in the architecture of peripheral substitution (either C_m-aryl or C_b-alkyl) have been studied in detail with the ground state absorption spectroscopy and density functional theory calculations. The geometry optimization, molecular orbitals and absorption spectra calculation have been carried out. It was found that protonation leads to the saddle type macrocycle conformation in contrast with the wave type conformation known for the parent-free base corroles. The mean plane deviation parameter Δ23 for the macrocycle, pyrrole tilting angles and the degree of pyramidalization λ^2 of all four pyrrole nitrogens was found to depend on the peripheral substitution architecture. Macrocycle conformation of the protonated forms has distinct asymmetrical features which are reflected by the sets of values of the tilting angles and values of pyramidalization degree. The pair of pyrroles B and C has smaller tilting angles and higher pyramidalization degree values, whereas the opposite trend was found for the pair of pyrroles A and D. Electronic effects and structural differences induced by substitution lead to the pronounced shifts of the molecular orbitals. In the C_b-alkylated corrole, almost-degenerated HOMO and HOMO-1 molecular orbitals lead to enhancement of the configuration interaction. As a result, the Q_x transition oscillator strength goes down, becoming comparable to that of the Q_y one. A large HOMO-HUMO-1gap in the C_m-aryl corrole minimizes the configuration interaction, giving rise to Q_x band domination in the visible range spectrum.

Keywords: free base corrole; protonation; macrocycle; substitution; pyramidalization; absorption spectrum; molecular orbitals

check for updates

Citation: Gladkov, L.L.; Klenitsky, D.V.; Kruk, M.M. Absorption Spectra of Protonated Corroles: Two Distinct Patterns Due to Peripheral Substitution Architecture. *Organics* **2023**, *4*, 490–502. https://doi.org/10.3390/org4040034

Academic Editor: Maurizio D'Auria

Received: 3 May 2023
Revised: 29 May 2023
Accepted: 13 July 2023
Published: 9 October 2023

Copyright: © 2023 by the authors. Licensee MDPI, Basel, Switzerland. This article is an open access article distributed under the terms and conditions of the Creative Commons Attribution (CC BY) license (https://creativecommons.org/licenses/by/4.0/).

1. Introduction

The concept of the conformational flexibility of tetrapyrrolic macrocycles and elucidation of the role of conformational control in carrying out their functions in natural and artificially designed systems became the working tool of knowledge in porphyrin chemistry [1,2]. While the general understanding of the problem has been achieved, plenty of particular tasks in this area are still waiting to be considered. Thus, an increasing interest in the free base tetrapyrrolic macrocycles with nonplanar molecular conformation has been noticed during the last decade [3], due to the perspective to use both the *amine*- and *imine*-nitrogens of pyrrolic fragments in the intermolecular reactions and hydrogen bonding. The idea underlying this interest is the perturbation of the macrocyclic core in nonplanar porphyrins, resulting in the exposure of pyrrolic nitrogens out of the macrocycle plane due to the pyrrole ring(s) tilting, which makes pyrrolic nitrogens easily accessible for interactions. Such a molecular conformation with an "active" macrocycle core can be easily achieved with either sterically demanding architecture of peripheral substitution, modification of the macrocyclic core itself by protonation of pyrrolenine *imine*-nitrogens or *N*-substitution [4–10]. The doubly protonated porphyrins bind efficiently ionic species

(either cationic or anionic, depending the porphyrin host structure) and are able to provide the selectivity of binding [3,11–13]. Nonplanar free base porphyrins and *N*-substituted porphyrins were found to reveal the catalytic activity [14]. Efficient H-bonding and anion binding has been also demonstrated for the other metal free porphyrinoids with contracted, expanded and *N*-confused macrocycles [15,16].

The distinct feature of the macrocycle of the free base corroles is the intrinsic nonplanarity, which originates from contraction of macrocycle which is lacking of one methine bridge and two adjacent pyrrole rings are connected by a C_a-C_a bond. As a result, the macrocycle consists of three pyrroles and one pyrrolenine ring to maintain its aromatic character and there are three protons in the macrocycle core. Three protons cannot reside in the tetrapyrrolic macrocycle plane due to the steric interactions which lead to deviations from the planar structure of the macrocycle, even in the absence of any other perturbation factors [17]. Because of three protons in the asymmetric macrocycle core, the free base corroles always exist as NH tautomers, differing in the arrangement of protons. Taken together, these peculiarities determine the integrated scheme of the acid–base and tautomeric equilibria in the free base corroles (Scheme 1), and dual channels with distinctly different equilibrium constants are proved experimentally for both protonation and deprotonation [18,19]. These features make the free base corroles very attractive compounds to provide the fine tuning of the acidity and basicity of the macrocycle core, and deserve to be subject of the fundamental study.

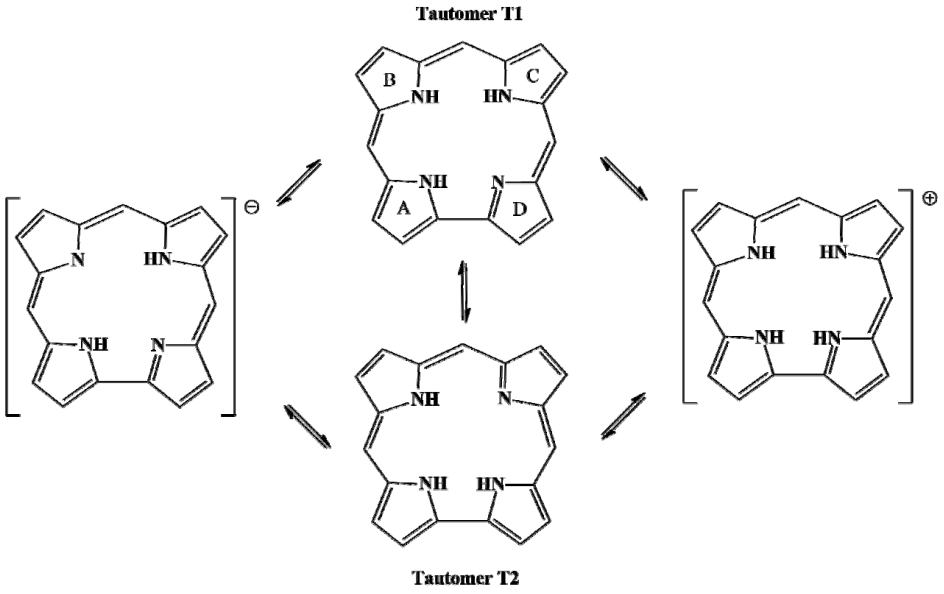

Scheme 1. The acid–base and NH-tautomeric equilibria of the free base corroles. The pyrrole rings notation (by capital letters) is shown at the structure of the tautomer T1. Arrows indicate the equilibria between the individual species (see text for detail).

Aimed to establish the relationship of the macrocycle basicity and the architecture of the peripheral substitution, and elucidate the spectral-luminescent properties of the protonated corroles, we have started the comparative study of two corroles differing with the pattern of peripheral substitution; namely, 2,3,7,13,17,18-hexamethyl-8,12-di-*n*-butylcorrole (hereinafter referred as H_3OAlkCor) and 10-(4,6-dichloro-pyrimidinyl)-5,15-dimesitylcorrole (hereinafter $H_3PyrMes_2Cor$) (Figure 1). The ground state absorption spectra of the protonated forms of these two corroles (hereinafter $H_4OAlkCor^+$ and $H_4PyrMes_2Cor^+$, respectively) reveal huge qualitative differences. The origin of these spectral differences is the subject of study in this work.

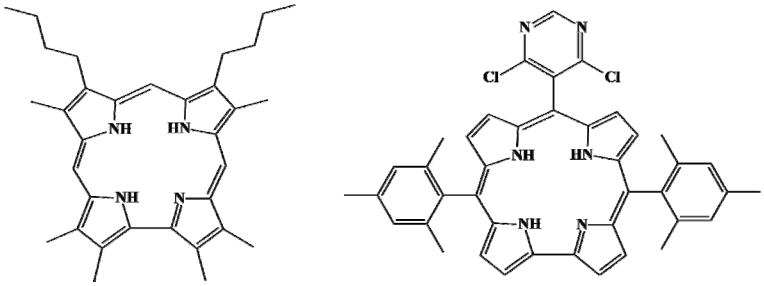

Figure 1. Molecular structure (as T1 tautomers) of the H_3OAlkCor(**left**) and the H_3PyrMes$_2$Cor (**right**).

2. Materials and Methods

The 2,3,7,13,17,18-hexamethyl-8,12-di-*n*-butylcorrole and10-(4,6-dichloropyrimi- dinyl)-5,15-dimesityl-corrole derivatives used in the study were prepared and purified according to the original synthetic procedures [20,21]. The working solutions were prepared by dissolving the corrole powder in organic solvents. The solutions' concentrations were determined according to spectrophotometry, using known extinction coefficients and have not exceeded 1×10^{-5} M, to avoid the aggregation effects. All of the solvents dichloromethane (DCM), dimethylsylfoxide (DMSO), acetonitrile (MeCN), ethanol (EtOH) and tetrahydrofuran (THF) were purchased from Aldrich (spectroscopic grade) and have been used as received. Electronic absorption spectra of the solutions were recorded on a CM 2203 two-in-one fluorescence spectrometer (ZAO Solar, Belarus). The experiments used standard quartz cuvettes (1×1 cm) placed into the temperature-controlled cuvette compartment of the instrument. The built-in thermostat allows it to keep the sample temperature in the range +5–+60 °C with an accuracy of ±0.5°.

Molecular geometries of the protonated corroles H_4OAlkCor$^+$ and H_4PyrMes$_2$Cor$^+$ in the ground electronic S_0 state were calculated using density functional theory with exchange-correlated functional PBE and three-exponential basis set at 3*z*, implemented by the quantum-chemical calculation program suite PRIRODA-04 [22,23]. The molecular geometry of artificial unsubstituted H_4Cor$^+$ has been also optimized to be used as a reference compound when analyzing the role of substitution patterns. The spectra of normal modes were calculated after optimizing the geometries, and the absence of imaginary frequencies for vibrational modes served as the criterion of reaching convergence. Optimization of the molecular conformation of tetrapyrrolic macrocycles with the density functional theory takes into account the electronic correlation and makes it possible to obtain the adequate values of bond lengths, which are consistent with the values obtained by the X-ray diffraction analysis [1]. For the optimized structure, the energy of the ground state and the energies of molecular orbitals were calculated, and the bond lengths and bond angles between the skeletal atoms of the macrocycle were determined. Electronic absorption spectra were calculated for the optimized molecular structures with the semi-empirical ZINDO/S method providing reasonable correlation with the experiment.

The nitrogen atom pyramidalization was estimated with the hybridization degree λ^2 value [24], which was calculated according to Equation (1):

$$1 + \lambda^2 \cos\theta = 0, \quad (1)$$

where θ is the arithmetic mean of the values of three angles between the directions of the bonds of the pyrrolic nitrogen with neighboring atoms: θ (C_aNC_a) and two θ (C_aNH).

To characterize the non-planar distortions of the contracted corrole macrocycle containing 23 skeletal atoms, the mean plane deviation parameter Δ23 (MPD Δ23) was introduced by analogy with MPD Δ24 for the porphyrin macrocycles [7]:

$$\Delta 23 = \sqrt{\frac{1}{23} + \sum_{i=1}^{23} \Delta z_i^2}, \quad (2)$$

where Δz_i is deviation an *i*-th skeletal from the macrocycle mean plane.

3. Results and Discussion

3.1. Ground State Absorption Spectra

The ground state absorption spectra of the protonated corroles $H_4OAlkCor^+$ and $H_4PyrMes_2Cor^+$, along with their free bases $H_3OAlkCor$ and $H_3PyrMes_2Cor$, are shown in Figure 2. The spectra of the free base corroles solutions have been explained earlier as a result of superimposing of the individual spectra of two NH-tautomers [25,26], with the long wavelength absorption $Q_x(0,0)$ bands belonging to each of two tautomers, which are indicated in italics (610.0 and 592.0 nm, respectively, for tautomers T1 and T2 of $H_4OAlkCor^+$, and 635.0 and 599.0 nm, respectively, for tautomers T1 and T2 of $H_4PyrMes_2Cor^+$). The spectra of the free base corrole tautomers with C_b-alkyl or C_m-aryl substitution was found to differ in the quantitative manner only [26]. On the contrary, the ground state absorption spectra of their protonated forms reveal two different patterns. Thus, the spectrum of the $H_4OAlkCor^+$ (Figure 2a) has two bands in the visible range of about the same intensity with corresponding maxima at 602 and 579.5 nm. The difference in the transition energies of two bands relates to the difference in the energies of two excited states, since the absorption takes place from the ground electronic state. Therefore, the energy gap between these two excited states amounting at 645 cm^{-1} can be evaluated. Since the long wavelength absorption at 602 nm should be univocally assigned to the pure electronic $Q_x(0,0)$ band, the energy gap is too small to assign the vibronic origin to the band peaking at 579.5 nm. Thus it should be considered as the band $Q_y(0,0)$ belonging to the second pure electronic transition $S_0 \rightarrow S_2$, since the asymmetry of the corrole macrocycle keeps out two of the lowest electronic states to degenerate, as it takes place in the case of symmetrically substituted doubly protonated porphyrins [27]. It should be pointed out that these bands are shifted hypsochromically compared to the band of the free base long wavelength tautomer T1, having a weak maximum at 610 nm. The weak diffuse absorption in the range 500–580 nm is due to overlapping vibronic absorption bands.

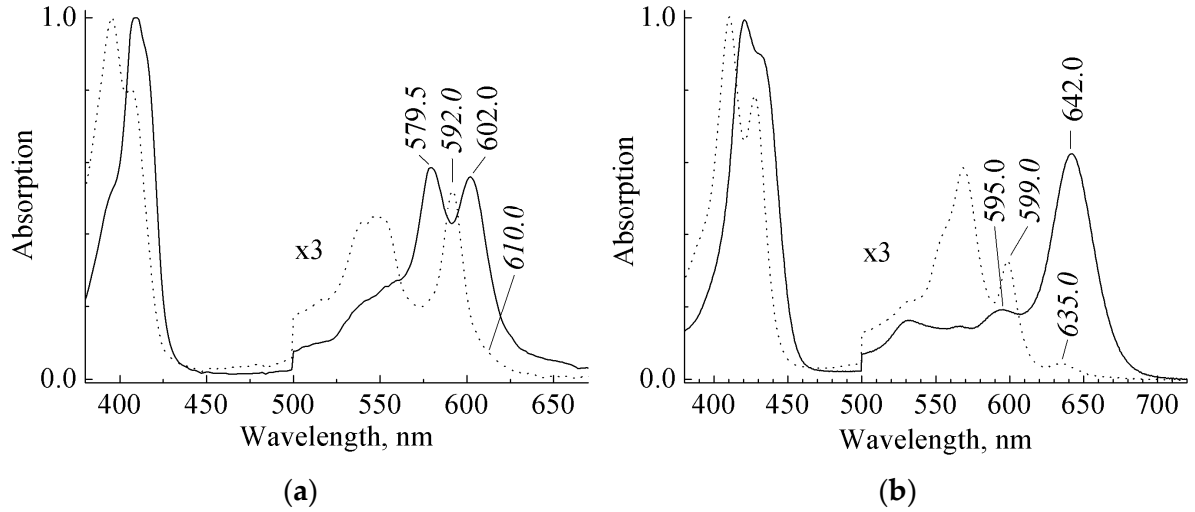

Figure 2. The ground state absorption spectra of the protonated corroles (solid line, maxima in regular): (**a**) $H_4OAlkCor^+$ in EtOH; (**b**) $H_4PyrMes_2Cor^+$ in THF. The corresponding free bases $H_3OAlkCor$ and $H_3PyrMes_2Cor$ spectra are shown for comparison (dotted line, maxima in italic). Spectra are normalized for the Soret band intensity and multiplied by factor 3 in the range above 500 nm for sake of clarity.

The strong absorption band with a maximum at 642 nm dominates in the spectrum of the $H_4PyrMes_2Cor^+$ and should be assigned as the pure electronic $Q_x(0,0)$ band (Figure 2b). This band has a bathochromic shift compared to the $Q_x(0,0)$ band of the free base long wavelength tautomer T1, with a maximum at 635 nm. The energy gap between the lowest S_1 electronic state of the $H_4PyrMes_2Cor^+$ and the next one, corresponding to absorption at 595 nm, is 1050 cm^{-1} only. Suggesting a more distorted molecular conformation for the C_m-aryl substituted protonated corroles, as it is for the doubly protonated porphyrins [5,28], this band should be assigned as the pure electronic $Q_y(0,0)$ band. Thus, the substitution architecture dramatically affects the spectra of protonated corroles, and the origin of differences needs to be clarified.

3.2. Macrocycle Conformation

Optimization of the molecular geometry of the protonated corroles reveals that the macrocycle adopts the saddle type conformation with pyrrole rings alternatively tilted up and down relative to the macrocycle mean plane, which was chosen as a plane passing through all three of the meso carbons, i.e., the $C_5C_{10}C_{15}$ plane. Eschenmoser diagrams (Figure 3) show the deviation of the skeletal atoms from the macrocycle mean plane. The analysis of skeletal deviations shown at Figure 3 and the structural data summarized in Table 1 allow conclusions about the molecular conformation in detail. First of all, it should be stressed that the average macrocycle nonplanarity estimated with the mean plane deviation parameter Δ23 differs noticeably for all three optimized structures. The minimum of the Δ23 value of 0.226 Å was found for unsubstituted H_4Cor^+, C_b-alkylation induces rising of the Δ23 value up to 0.247 Å, and C_m-aryl substitution doubles this difference, so theΔ23 value amounts to 0.265 Å. These values support the above suggestion on the different degree of macrocycle nonplanarity based on the analysis of $\Delta E(S_2–S_1)$ splitting.

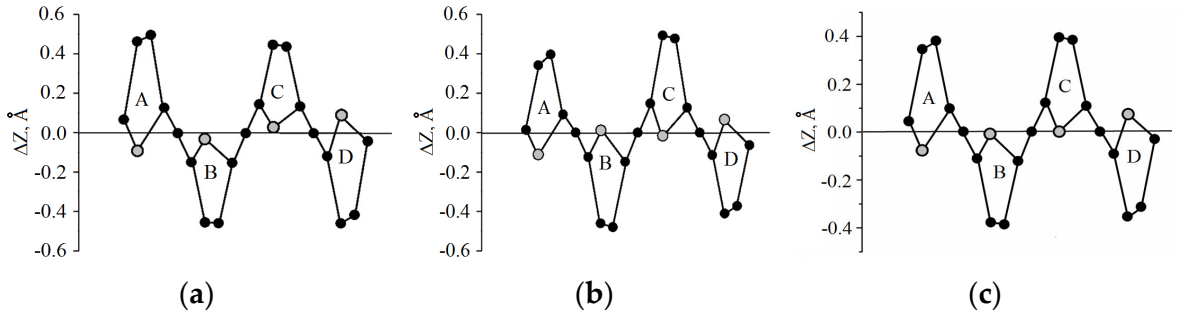

Figure 3. Linear display of the skeletal atoms deviations from the macrocycle mean plane in the protonated corroles: (**a**) $H_4OAlkCor^+$; (**b**) $H_4PyrMes_2Cor^+$; (**c**) H_4Cor^+. To distinguish the nitrogen atoms the corresponding circles are grey colored. Capital letters refer to the particular pyrrole rings as indicated at Figure 1.

Table 1. Parameters of conformation of the protonated corrole macrocycles (see text for detail).

Molecule	Δ23,Å	φ(A),°	φ(B),°	φ(C),°	φ(D),°	C_1–C_{19},Å
$H_4OAlkCor^+$	0.247	14.4	9.9	9.8	13.5	1.428
$H_4PyrMes_2Cor^+$	0.265	13.6	12.9	13.5	12.8	1.427
H_4Cor^+	0.225	12.5	10.0	10.4	11.7	1.424

Upon protonation, the average increase in the mean plane deviation parameter Δ23 is smaller for the C_m-aryl substituted corrole (0.2 Å → 0.265 Å) compared to the C_b-alkylated one (0.16 Å → 0.245 Å). Since both NH tautomers of $H_3PyrMes_2Cor$ are known to have the wave type molecular conformation [25,29], the saddle conformation of the protonated $H_4PyrMes_2Cor^+$ implies that wave-to-saddle conformational transition takes place for this molecule. On the contrary, two NH-tautomers of the free base $H_3OAlkCor$ have

different types of nonplanar distortion: tautomer T1 has wave-type distortion, whereas the dominating tautomer T2 possesses the saddle-type macrocycle [29]. Based on close values of the C_1–C_{19} bond length in the protonated $H_4OAlkCor^+$ and in tautomer T2 of the free base $H_3OAlkCor$, one can expect that the saddle conformation of the protonated corrole would resemble some features of the parent-free base T2 tautomer.

When comparing the pyrrolic nitrogen positions in the $H_4OAlkCor^+$ and $H_4PyrMes_2Cor^+$, one can conclude that, in the latter, they find themselves alternatively down-up-down-up relative to the mean macrocycle plane, whereas in the former, a down-down-up-up pattern is observed. Therefore, in the $H_4OAlkCor^+$, the couple of nitrogens N_{21} and N_{22}, lie under the mean plane, and the nitrogens N_{23} and N_{24} lie above it, resulting in the asymmetrical stair-like arrangement which enhances the nitrogen's repulsion. In the $H_4PyrMes_2Cor^+$, such repulsion is minimized due to the more symmetrical nitrogen arrangement.

In relation to the early theoretical study of protonated C_m-aryl substituted corroles [30], where the existence of two conformers with energy separation 15.8–18.5 kJ/mol have been suggested, one must state that any spectral evidences of the heterogeneity in the solutions of protonated corroles was not found. This statement is in line with our earlier study [18], where no temperature activation was observed in the solutions of protonated corroles, up to temperatures 333 K.

The tilting angles were found to be different for the pairs of pyrroles A and D, and B and C in $H_4OAlkCor^+$ and H_4Cor^+ (Table 1). In the dipyrromethene fragment (pyrroles B and C) the φ is about 10° for both compounds, whereas in the dipyrrole fragment (pyrroles A and D) it increases for ~2° in H_4Cor^+ and ~4° in $H_4OAlkCor^+$. The dipyrromethene-to-dipyrroletilting angle φ difference indicates the asymmetry of saddling, and the increase in tilting angle in the $H_4OAlkCor^+$ results from the sterical hindrances due to the interaction of methyl groups in the C_2 and C_{18} positions of pyrroles A and D.

This sterical repulsion is evidenced also in the C_1-C_{19} bond length increase in going from the unsubstituted H_4Cor^+ corrole to the $H_4OalkCor^+$, and in moving of methyl substituents in the C_2 and C_{18} positions out of the pyrrole plane due to steric repulsion (torsion angles $N_{24}C_{19}C_{18}C_{Me}$ and $N_{21}C_1C_2C_{Me}$ increase). Introducing the sterically demanding 4,6-dichloropyrimidinyl and mesityl rings in the C_m-positions of the macrocycle leads to an increase in the tilting angles, but at the same time makes them more evenly distributed. A different source of tilting angle increase in the $H_4PyrMes_2Cor^+$ is reflected by a decrease in the C_1-C_{19} bond length, compared to the $H_4OAlkCor^+$ (see Table 1).

The *amine* nitrogens of the free base corrole is known to undergo pyramidalization with the pattern differing between two NH-tautomers [19]. The Driving force for the pyramidalization is the same as for the pyrrole tilting; namely, the steric repulsion of NH groups in the macrocycle core. The Coulomb repulsion force adds to steric repulsion in the protonated corrole, leading to increase both the pyrrole tilting and pyrrole nitrogen pyramidalization. Based on the optimized molecular structures of protonated corroles, we quantified the pyramidalization with the hybridization degree λ^2 values (Table 2).

Table 2. Hybridization degree λ^2 of the pyrrole nitrogens calculated with Equation (1).

Molecule	N_{21}(pyrrole A)	N_{22}(pyrrole B)	N_{23}(pyrrole C)	N_{24}(pyrrole D)
$H_4OAlkCor^+$	2.228	2.306	2.300	2.225
$H_4PyrMes_2Cor^+$	2.166	2.297	2.289	2.154
H_4Cor^+	2.202	2.297	2.293	2.203

Analysis of the calculated λ^2 values stresses the macrocycle conformation asymmetry once again. In all three protonated macrocycles, different pyramidalization was found in the dipyrromethene and dipyrrole fragments. The remarkable feature is that pyrroles B and C in the dipyrromethene fragment of all three protonated corroles reveal essentially the same λ^2 values, ~2.3. Such a behavior prevents the simplified explanation that tilting angle and pyramidalization can change one at the expense of the other. Pyrrole tilting varies noticeably, but the pyramidalization does not change. On the contrary, the hybridization

degree λ^2 values for the pyrroles A and D in the dipyrrole fragment reveal adistinct trend related to the substitution pattern. The λ^2 value of ~2.2 was calculated for the unsubstituted protonated H_4Cor^+ corrole. The hybridization degree λ^2 increases upon C_b-alkylation up to ~2.23, but decreases down to ~2.16 upon C_m-aryl substitution. Again, the reciprocal relationship with the tilting angle value is invalid. Therefore, one can conclude that nonplanar distortions in the dipyrromethene fragment of the protonated macrocycle are larger. Taking into account the recently reported relationship of the hybridization degree λ^2 and π-conjugation pathway through the pyrrole ring [31], one can suggest that the outer branch in the dipyrromethene fragment (via C_b-positions) should have excess of the electron density and the π-conjugation pathway is pushed to the macrocycle periphery. A smaller hybridization degree λ^2 of the nitrogens in the dipyrrole fragment allows a less different proportion of the π-conjugation macrocyclic currents via the inner and outer branches of the pyrrolic ring. The inner part of the dipyrrole fragment will have higher electronic density compared to the inner part of the dipyrromethene fragment, giving rise to the gradient electric field in the macrocycle core.

3.3. Molecular Orbitals Calculations

The molecular orbitals of the protonated corroles were calculated with the DFT method, and Figure 4 shows the four Gouterman molecular orbitals which are known to be determinative for the absorption spectra of tetrapyrrolic compounds [32]. One can see that the substitution architecture and the induced structural differences give rise to the alterations of the electronic density distribution over the macrocycle. Thus, the least differences among the studied derivatives are observed for the lowest unoccupied molecular orbitals, LUMO and LUMO+1. However, distinctly smaller amount of the electronic density appears at the pyrrolic nitrogens N_{22} and N_{23} for the LUMO+1 molecular orbital of both substituted derivatives, compared to that of the unsubstituted protonated H_4Cor^+ corrole, with it is practically vanishes in case of the $H_4PyrMes_2Cor^+$. The shape of the LUMO orbitals is about the same for the unsubstituted derivative H_4Cor^+ and the $H_4OAlkCor^+$, but the nodes are observed at the pyrrolic nitrogens N_{22} and N_{23} for the $H_4PyrMes_2Cor^+$.

The highest occupied molecular orbitals HOMO and HOMO-1 orbitals demonstrate completely different behavior. The HOMO and HOMO-1 orbital patterns of the unsubstituted H_4Cor^+ can be found in the $H_4PyrMes_2Cor^+$ macrocycle, but their ordering is reversed. This is evidenced by the same pattern of distribution of electronic density in the macrocycle, when the nodes and antinodes locate at the same atoms/bonds. Thus, the "a_{1u}-like" orbital (in the D_{4h} symmetry group notation) is the HOMO for the unsubstituted H_4Cor^+ macrocycle, but it appears as HOMO-1 for the $H_4PyrMes_2Cor^+$. On the contrary, "a_{2u}-like" orbital is the HOMO-1 for the H_4Cor^+, but the HOMO for the $H_4PyrMes_2Cor^+$. Therefore, the molecular orbital shifts can be argued about in the case of C_m-aryl substitution.

But, it is not the case for the C_b-alkyl substitution, where the orbital mixing takes place. Each of the HOMO and HOMO-1 orbitals bear the features of both the highest occupied molecular orbitals of the unsubstituted H_4Cor^+. These orbitals seem to be similar to each other and can be interexchanged with reflection, relative to the plane orthogonal to the macrocycle plane and passing through the carbon C_5 and the middle of the C_1-C_{19} bond. These features resemble those of two degenerated lowest unoccupied molecular orbitals in the porphine, e_{gx} and e_{gy}. Thus, one can suggest the HOMO and HOMO-1 orbitals of the $H_4OAlkCor^+$ are very close in energy. Indeed, the calculated molecular orbital energies, plotted on Figure 5, confirm that it is the case.

The energy difference between the HOMO and HOMO-1 of the $H_4OAlkCor^+$ is 970cm^{-1} (0.120 eV). This value is much smaller compared to 2220 cm^{-1} (0.275 eV) and 1790cm^{-1} (0.221 eV) for the $H_4PyrMes_2Cor^+$ and H_4Cor^+, respectively. The small energy difference between the HOMO and HOMO-1 provides the conditions for the efficient configuration interaction. The configuration interaction of two electronic transitions has the maximum value in case the transition energy degenerates, i.e., when the molecular orbitals involved in their formation are of the same energy. According to the Gouterman

model [32], when the configuration interaction increases due to a decrease in the energy difference between the HOMO and HOMO-1, the absorptivity of the lowest electronic transition $Q_x(0,0)$ is expected to drop. This is the case for the H_4OAlkCor$^+$. On the contrary, large detuning of orbitals in the H_4PyrMes$_2$Cor$^+$ diminishes the configuration interaction and the long wavelength band absorptivity increases. Thus, the molecular orbital energy calculations provide the basis to explain the experimentally observed spectral differences.

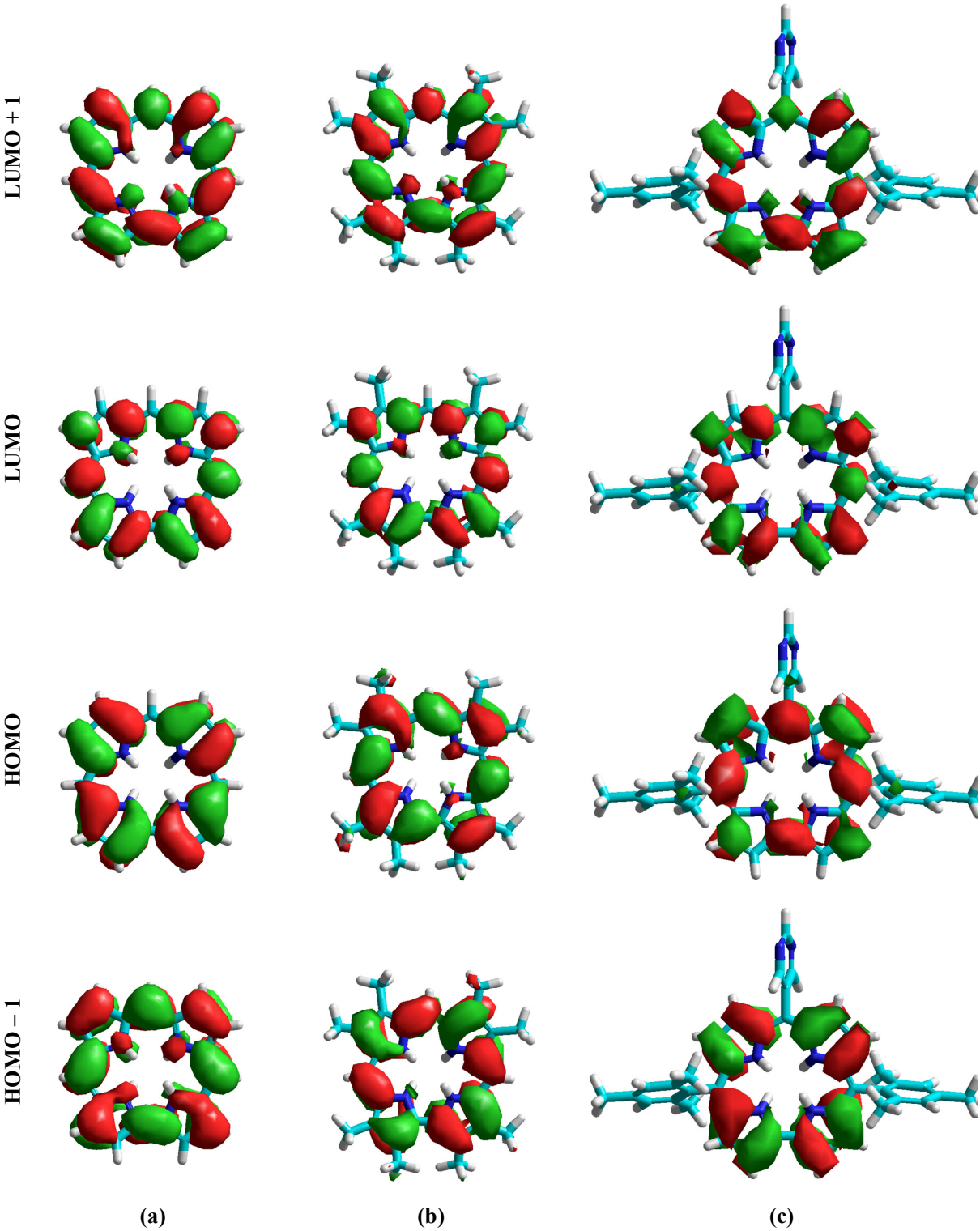

Figure 4. The four Gouterman molecular orbitals of the protonated corroles: (**a**) H_4Cor$^+$; (**b**) H_4OAlkCor$^+$; (**c**) H_4PyrMes$_2$Cor$^+$.

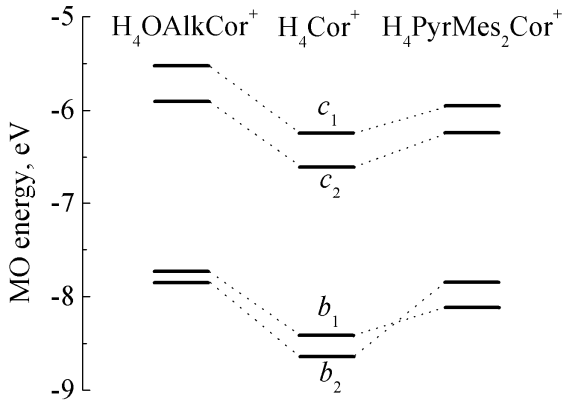

Figure 5. The four Gouterman molecular orbital energy plots for the protonated corroles.

3.4. Calculations of the Absorption Spectra

To reassure the suggested interpretation, the ground state absorption spectra(both the transition wavelengths and the oscillator strengths) were calculated with the ZINDO/S method. ZINDO/S spectra calculations, taken with the molecular structure optimized with the DFT method, were proved to allow for tetrapyrrolic macrocycles a good correlation with the experiment with the minimum need for computational time [1]. The results of the calculations are summarized in Table 3.

Table 3. The maxima of two lowest electronic transition bands and the corresponding oscillator strengths for the protonated corroles.

Molecule	$Q_x(0,0)/Q_y(0,0)$, nm	f_x/f_y
H4OAlkCor$^+$	676.0/632.2	0.060/0.045
H4PyrMes2Cor$^+$	669.6/589.0	0.115/0.005
H4Cor$^+$	666.4/634.1	0.047/0.032

The calculated spectrum for the $H_4PyrMes_2Cor^+$ demonstrates good reproducibility of both band positions and oscillator strengths in the experimental spectrum. Due to domination of the oscillator strength of the $Q_x(0,0)$ band the theoretical spectrum has a single band feature as it was found in the experiment. The theoretical band position maxima of the $H_4OAlkCor^+$ are bathochromically shifted relative to the experimental one. One can suggest that this overestimation of the wavelength maxima is likely due to the HOMO and HOMO-1 orbital mixing, as was evidenced above. However, the oscillator strengths *f* is reproduced nicely for both transitions, and they are of comparable intensity, as it is found in the experimental spectrum.

The calculated oscillator strengths for the H_4Cor^+ are in line with these observations. The proportion of the oscillator strengths lies in between the two above cases, in agreement with the intermediate value of the energy difference of HOMO and HOMO-1 orbitals. Thus, one can conclude that the oscillator strength of the long wavelength transition of the $H_4OAlkCor^+$ decreases due to an increased configuration interaction, leading to formation of both absorption bands with comparable intensity. On the contrary, a decrease in the configuration interaction in the $H_4PyrMes_2Cor^+$ enables the domination of the long wavelength transition.

3.5. Tuning the Configuration Interaction with Specific Solvation

The protonated form of the $H_4OAlkCor^+$ was studied in the series of solvents with different properties: dichloromethane (DCM) is a nonpolar aprotic solvent; dimethylsylfoxide (DMSO) and acetonitrile (MeCN) are polar aprotic solvents; and ethanol (EtOH) is a polar protic solvent. The aim of the studies is to inspect the solvatochromic shifts of

two absorption bands and verify the band assignment. The protonated form was achieved in all of the cases and the spectra have been measured (Figure 6).

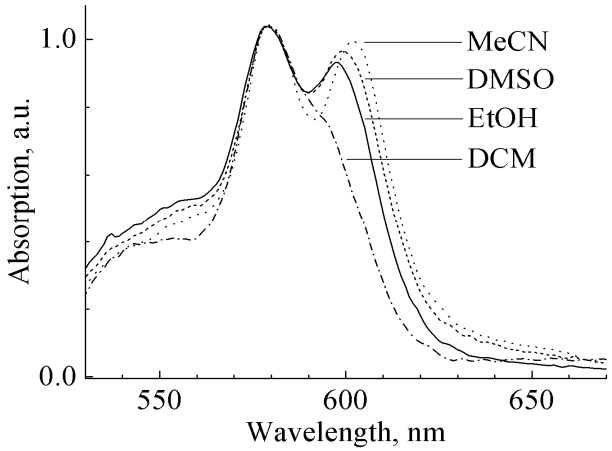

Figure 6. The ground state absorption spectra of the $H_4OAlkCor^+$ in visible wavelength range as a function of solvent.

The solvent dependence was found to differ for two bands. This finding supports the assignment of these bands to two different electronic transitions. If the high frequency band would be of vibronic origin, it should follow the solvent shift of the parent electronic band, but this is not the case.

The $Q_x(0,0)$ band undergoes a noticeable shift with the solvent change, whereas the position of the $Q_y(0,0)$ band remains practically unchanged. Such a difference can be explained when the general and specific solvent effects take place simultaneously [33]. The latter is likely to be the hydrogen-bonding interactions in the macrocycle core, which take place for the protonated tetrapyrrolic macrocycles [4,5]. One more feature can be seen in the spectra: the intensity of the $Q_x(0,0)$ band increases as its maximum shifts bathochromically. Keeping in the mind that $Q_y(0,0)$ band does not shift, this observation means that the intensity increase parallels the increase in the energy gap between two electronic transitions. This finding supports the suggested role of the configuration interaction in the formation of the spectral pattern. Indeed, the increase in the energy gap originates from the molecular orbitals detuning, which, in its own turn, decreases the configuration interaction.

4. Conclusions

The ground state absorption spectra of two protonated corroles differing in the architecture of peripheral substitution have been studied in detail. The C_m-aryl substitution leads to the formation of one strong absorption band in the visible range, which has a bathochromic shift compared to the position of the long wavelength band of the corresponding free base corrole. On the contrary, the C_b-alkylated derivative demonstrates two absorption bands of about the same intensity, with the long wavelength transition having a hypsochromic shift compared to that of the corresponding free base. Both studied corroles adopt the saddle-type macrocycle distortions upon protonation, with the pyrrole tilting angles φ being higher for the C_m-aryl-substituted derivative. The mean plane deviation parameter Δ23 is 0.265 and 0.247 Å for the C_m-aryl and C_b-alkylated corroles, respectively. The saddling magnitude was found to parallel the trend observed for doubly protonated porphyrins; namely, the C_m-aryl substituted derivative, which revealed higher tilting angles compared to those in the C_b-alkylated one. However, in contrast with doubly protonated symmetrically substituted porphyrins, where tilting angles are the same, the φ angles are higher for the pyrroles A and D in the bipyrrole unit, compared to those for pyrroles B and C in the pyrromethene fragment. Comparison with the unsubstituted protonated corrole model allows us to suggest that this difference is intrinsic, but in the case of the C_b-alkylated corrole, the tilting angle increases additionally due to the steric hindrances of

methyl groups attached to the C_2 and C_{18} positions. All of the pyrrole nitrogens undergo substantial pyramidalization upon protonation. The degree of pyramidalization λ^2 was found to be higher for the pyrroles B and C in the dipyrromethene fragment, compared to those for pyrroles A and D in the bipyrrole unit. The difference in λ^2 values between two pairs of pyrroles is smaller for the C_b-alkylated derivative, leading to a more symmetrical molecular conformation. All of these structural differences result in alterations of the electronic structure of the two studied corroles. While the LUMO and LUMO+1 molecular orbitals are not too different in the shape, the HOMO and HOMO-1 orbitals demonstrate completely different pictures of wavefunction nodes/antinodes in the macrocycle. Moreover, these orbitals practically degenerate in the C_b-alkylated derivative, giving rise to a huge increase in the configuration interaction, which, in its own turn, leads to the reducing of absorptivity of the long wavelength electronic transition. A smaller energy gap between the Q_x and Q_y bands in the C_b-alkylated corrole (645 cm^{-1}), compared to that in the C_m-aryl corrole (1050 cm^{-1}), indicates that the former has the higher symmetry. As a result of the increased configuration interaction in the C_b-alkylated corrole, the oscillator strength of the long wavelength transition decreases, producing two absorption bands of comparable intensity, whereas the long wavelength absorption band Q_x dominates over the Q_y band in the spectrum of the C_m-aryl corrole.

The protonated forms of corroles are of increasing interest as basic compounds for the design of luminescent sensors. Therefore, any way to tune sensitivity or improve the performance is of importance. We suggest that spectral features are fruitfully analyzed with the concept of multicenter interactions when the overall molecular response is due to interplay, frequently in the nonlinear manner, of individual molecular fragments, or even individual atoms like the pyrrole nitrogens, whose pyramidalization was shown to serve as the gate to arrange the π-conjugated macrocycle pathway. Concerning the pyrrole nitrogen pyramidalization, its role in the formation of the electronic structure of nonplanar macrocycles is underestimated, especially of those having the contracted macrocycle. The anion sensing with either an *N*-pyrrole-modified or protonated macrocycle core is also mediated with pyrrole pyramidalization. Our recent finding is that *N*-substitution induced a bathochromic shift in porphyrin and it is almost completely due to the nitrogen pyramidalization, rather than to the substituted pyrrole tilting, as was expected traditionally [34]. Future research in this direction is in progress.

Author Contributions: Conceptualization, M.M.K. and L.L.G.; methodology, M.M.K.; software, L.L.G.; validation, L.L.G., D.V.K. and M.M.K.; formal analysis, L.L.G. and D.V.K.; investigation, M.M.K.; resources, L.L.G.; data curation, L.L.G.; writing—original draft preparation, M.M.K.; writing—review and editing, M.M.K.; visualization, M.M.K. and D.V.K.; supervision, M.M.K.; project administration, M.M.K.; funding acquisition, M.M.K. All authors have read and agreed to the published version of the manuscript.

Funding: This research was funded by the Republic of Belarus State Fundamental Research Program "Convergence-2025", Subprogram "Interdisciplinary Research and New Emerging Technologies", Grant 3.03.10.2. M.K. also acknowledges for the personal grant from the President of the Republic of Belarus.

Data Availability Statement: No additional new data were created.

Acknowledgments: Authors express their gratitude to W. Dehaen (Katolic University of Leuven, Belgium), W. Maes (University of Hasselt, Belgium), D.V. Petrova (Institute of Physics of Microstructures of RAS, Nijnii Novgorod, Russia) and A.S. Semeikin (Ivanovo State University of Chemistry and Technology, Russia) for providing the free base corroles for this study.

Conflicts of Interest: The authors declare no conflict of interest.

References

1. Senge, M.O. The conformational flexibility of tetrapyrroles—Current model studies and photobiological relevance. *J. Photochem. Photobiol. B Biol.* **1992**, *16*, 3–36. [CrossRef]
2. Senge, M.O.; MacGovan, S.A.; O'Brien, J. Conformational control of cofactors in nature—The influence of protein-induced macrocycle distortion on the biological function of tetrapyrroles. *Chem. Commun.* **2015**, *51*, 17031–17063. [CrossRef]
3. Kielmann, M.; Senge, M.O. Molecular engineering of free-base porphyrins as ligands—The N-H. . .X binding motif in tetrapyrroles. *Angew. Chem. Int. Ed.* **2019**, *58*, 418–441. [CrossRef]
4. Stone, A.; Fleischer, E.B. The molecular and crystal structure of porphyrin diacids. *J. Am. Chem. Soc.* **1968**, *90*, 2735–2748. [CrossRef]
5. Cheng, B.; Munro, O.Q.; Marques, H.M.; Scheidt, W.R. An analysis of porphyrin molecular flexibility—Use of porphyrin diacids. *J. Am. Chem. Soc.* **1997**, *119*, 10732–10742. [CrossRef]
6. Lavallee, D.K. *The Chemistry and Biochemistry of N-Substituted Porphyrins*, 1st ed.; Wiley-VCH: New York, NY, USA, 1987; pp. 254–313.
7. Senge, M.O. Highly substituted porphyrins. In *The Porphyrin Handbook*, 1st ed.; Kadish, K.M., Smith, K.M., Guillard, R., Eds.; Academic Press: New York, NY, USA; World Scientific: Singapore, 2000; Volume 1, pp. 239–347.
8. Roucan, M.; Flanagan, K.J.; O'Brien, J.; Senge, M.O. Nonplanar porphyrins by N-substitution: A neglected pathway. *Eur. J. Org. Chem.* **2018**, *46*, 6432–6446. [CrossRef]
9. Fang, Y.; Bhyrappa, P.; Ou, Z.; Kadish, K.M. Planar and nonplanar free-base tetrarylporphyrins: β-pyrrole substituents and geometric effects on electrochemistry, spectroelectrochemistry, and protonation/deprotonation reactions in nonaqueous media. *Chem. Eur. J.* **2014**, *20*, 524–532. [CrossRef]
10. Ballester, M.; Ravotto, L.; Quirke, J.M.E.; Lopez de Vega, R.; Shelnutt, J.A.; Cheprakov, A.V.; Vinogradov, S.A.; Medforth, C.J. Protonation of planar and nonplanar porphyrins: A calorimetric and computational study. *J. Phys. Chem. A* **2020**, *124*, 8994–9003. [CrossRef]
11. Kruk, M.M.; Ivanova, Y.B.; Sheinin, V.B.; Starukhin, A.S.; Mamardashvili, N.Z.; Koifman, O.I. Highly sensitive halide ions recognition with diprotonated porphyrin. *Macroheterocycles* **2008**, *1*, 50–58. [CrossRef]
12. Kruk, M.M.; Starukhin, A.S.; Mamardashvili, N.Z.; Mamardashvili, G.M.; Ivanova, Y.B.; Maltseva, O.V. Tetrapyrrolic compounds as the hosts for binding of halides and alkali metal cations. *J. Porph. Phthal.* **2009**, *13*, 1148–1158. [CrossRef]
13. Novaritsa, K.; Flanagan, K.J.; Gibbons, D.; Senge, M.O. Conformational Re-engineering of porphyrins as receptors with switchable N-H. . .X-type binding modes. *Angew. Chem. Int. Ed.* **2019**, *58*, 16553–16557. [CrossRef]
14. Roucan, M.; Kielmann, M.; Connon, S.J.; Bernhard, S.S.R.; Senge, M.O. Conformational control of nonplanar freebase porphyrins: Toward bifunctional catalysts of tunable basicity. *Chem. Comm.* **2018**, *54*, 26–29. [CrossRef]
15. Ding, Y.; Zhu, W.-H.; Xie, Y. Development of ion chemosensors based on porphyrin analogues. *Chem. Rev.* **2017**, *117*, 2203–2256. [CrossRef]
16. Paolesse, R.; Nardis, S.; Monti, D.; Stefanelli, M.; Di Natale, C. Porphyrinoids for chemical sensor applications. *Chem. Rev.* **2017**, *117*, 2517–2583. [CrossRef]
17. Kruk, M.M.; Klenitsky, D.V.; Maes, W. Molecular structure and conformation of free base corroles. *Macroheterocycles* **2019**, *12*, 58–67. [CrossRef]
18. Ivanova, Y.B.; Savva, V.A.; Mamardashvili, N.Z.; Starukhin, A.S.; Ngo, T.H.; Dehaen, W.; Maes, W.; Kruk, M.M. Corrole NH Tautomers: Spectral Features and Individual Protonation. *J. Phys. Chem. A* **2012**, *116*, 10683–10694. [CrossRef]
19. Kruk, M.M.; Ngo, T.H.; Savva, V.A.; Starukhin, A.S.; Dehaen, W.; Maes, W. Solvent-Dependent Deprotonation ofmeso-Pyrimidinylcorroles: Absorption and Fluorescence Studies. *J. Phys. Chem. A* **2012**, *116*, 10704–10711. [CrossRef]
20. Ngo, T.H.; Puntoniero, F.; Nastasi, F.; Robeyns, K.; Van Meervelt, L.; Campagna, S.; Dehaen, W.; Maes, W. Synthetic, Structural, and Photophysical Exploration of meso-Pyrimidinyl-Substituted AB_2-Corroles. *Chem. Eur. J.* **2010**, *16*, 5691–5705. [CrossRef]
21. Petrova, D.V.; Semeikin, A.S.; Berezina, N.M.; Berezin, M.B.; Bazanov, M.I. Synthesis and Some Physical-Chemical Properties of meso-Aryl- and Alkyl Substituted Corroles and their Metal Complexes. *Macroheterocycles* **2019**, *12*, 119–128. [CrossRef]
22. Laikov, D.N. Fast evaluation of density functional exchange-correlation terms using the expansion of the electron density in auxiliary basis sets. *Chem. Phys. Lett.* **1997**, *281*, 151–156. [CrossRef]
23. Laikov, D.N.; Ustynyuk, Y.A. PRIRODA-04: A quantum-chemical program suite. New possibilities in the study of molecular systems with the application of parallel computing. *Russian Chem. Bull.* **2005**, *54*, 820–826. [CrossRef]
24. Alabugin, I.V.; Bresch, S.; Gomes, G.P. Orbital hybridization: A key electronic factor in control of structure and reactivity. *J. Phys. Org. Chem.* **2015**, *28*, 147–162. [CrossRef]
25. Beenken, W.J.D.; Presselt, M.; Ngo, T.H.; Dehaen, W.; Maes, W.; Kruk, M.M. Molecular Structures and Absorption Spectra Assignmentof Corrole NH Tautomers. *J. Phys. Chem. A* **2014**, *118*, 862–871. [CrossRef]
26. Ajeeb, Y.H.; Klenitsky, D.V.; Vershilovskaya, I.V.; Petrova, D.V.; Semeikin, A.S.; Maes, W.; Gladkov, L.L.; Kruk, M.M. Spectral and luminescent properties and NH-tautomerism of alkylated corrole free bases. *J. Appl. Spectr.* **2020**, *87*, 421–428. [CrossRef]
27. Kruk, M.M.; Starukhin, A.S.; Maes, W. Influence of macrocycle protonation on the photophysical properties of porphyrins. *Macroheterocycles* **2011**, *4*, 69–79. [CrossRef]
28. Rosa, A.; Ricciardi, G.; Baerends, E.J. Synergism of porphyrin-core saddling and twisting of *meso*-aryl substituents. *J. Phys. Chem. A* **2006**, *110*, 5180–5190. [CrossRef]

29. Klenitsky, D.V.; Gladkov, L.L.; Vershilovskaya, I.V.; Maes, W.; Kruk, M.M. Inversion of aromaticity of NH-tautomers of the free base corroles in the lowest triplet T_1 state. *J. Appl. Spectr.* **2022**, *89*, 426–432. [CrossRef]
30. Gao, H.-L.; Yao, G.-H.; Chen, F.; Wang, W.-L.; Chen, D.-M. Density Functional Theory Investigation of Structures and Electronic Spectra of N-protonated Corroles. *Chin. J. Chem. Phys.* **2012**, *25*, 281–290. [CrossRef]
31. Kruk, M.M.; Gladkov, L.L.; Klenitsky, D.V.; Krylov, A.B. Molecular conformation and aromaticity of N-substituted porphine derivatives. *Proc. BSTU Issue 3 Phys. Math. Inform.* **2023**, *266*, 34–41. (In Russian) [CrossRef]
32. Gouterman, M. Optical spectra and electronic structure of porphyrins and related rings. In *The Porphyrins*, 1st ed.; Dolphin, D., Ed.; Academic Press: New York, NY, USA, 1978; Volume 3, pp. 1–165.
33. Kruk, M.M. Solvatochromism of the free base corroles. *J. Appl. Spectr.* **2022**, *89*, 624–630. [CrossRef]
34. Gladkov, L.L.; Klenitsky, D.V.; Kruk, M.M. Mechanisms of bathochromic band shifts in the absorption spectra of the N-substituted porphine derivatives. *J. Appl. Spectr.* **2023**. [CrossRef]

Disclaimer/Publisher's Note: The statements, opinions and data contained in all publications are solely those of the individual author(s) and contributor(s) and not of MDPI and/or the editor(s). MDPI and/or the editor(s) disclaim responsibility for any injury to people or property resulting from any ideas, methods, instructions or products referred to in the content.